

Case Resolution

Rodrigo Re,^{*} Santiago L. Iglesias,^{**} Bartolomé L. Allende^{**}

^{*}Diagnostic Imaging Service, Osteoarticular/Musculoskeletal Area - Interventionism, Sanatorio Allende, Córdoba, Argentina

^{**}Orthopedics and Traumatology Service, Sanatorio Allende, Córdoba, Argentina

Case presentation on page 130.

DIAGNOSIS: Extrapulmonary sarcoidosis.

DISCUSSION

An infiltrative-looking lesion was visualized in the right hip magnetic resonance (Figure 3), at the level of the iliac bone, in the acetabular roof, heterogeneous, hypointense on the T1-weighted sequence and hyperintense on the T2-weighted sequence, with discrete hypersignal in diffusion sequences, associated with cortical thinning. It was accompanied by joint effusion at the coxofemoral level, with a heterogeneous signal, with capsular distension.



Figure 3. Magnetic resonance imaging of the right hip. **A.** Coronal section in T1-weighted sequence. A hypointense lesion is visualized in the roof of the acetabulum (arrow). **B.** Coronal section in STIR sequence. The lesion becomes hyperintense (arrow) and a heterogeneous hip effusion is observed (asterisk). **C.** Axial section in STIR sequence. Hyperintense lesion (arrow). **D and E.** Axial section in diffusion sequence (**D**) with the corresponding apparent diffusion coefficient map (**E**), showing intermediate cellularity.

Dr. RODRIGO RE • rodrigo_re@hotmail.com  <https://orcid.org/0000-0001-7382-9459>

How to cite this article: Re R, Iglesias SL, Allende BL. Postgraduate Orthopedic Instruction – Imaging. Case Resolution. *Rev Asoc Argent Ortop Traumatol* 2023;88(2):257-263. <https://doi.org/10.15417/issn.1852-7434.2023.88.2.1731>

With these radiological findings and the suspicion of a proliferative neoplastic process, other imaging studies and biochemical analyzes were requested.

Gynecological and mammary ultrasounds were performed, which did not reveal particularities. The mammogram was normal and the complete analysis with carcinoembryonic antigen, CA15.3 and alkaline phosphatase were normal.

The evaluation also included a positron emission tomography (Figure 4) that showed a lesion in the upper right lung lobe, with fibrous tracts and bronchiectasis associated with glucose hypermetabolism (SUVmax. 4.2). Also, an osteolytic lesion with disruption of the cortex and intense glucose hypermetabolism was visualized in the anterosuperior sector of the right acetabulum (SUVmax. 14.2). It was accompanied by annular morphology hypermetabolism surrounding the femoral head, which maintained its sphericity, suggesting a capsular pathology. In the external obturator muscle, between the ischium and the trochanter, a hypermetabolic hypodense image of 30 mm (SUVmax 11) was observed.

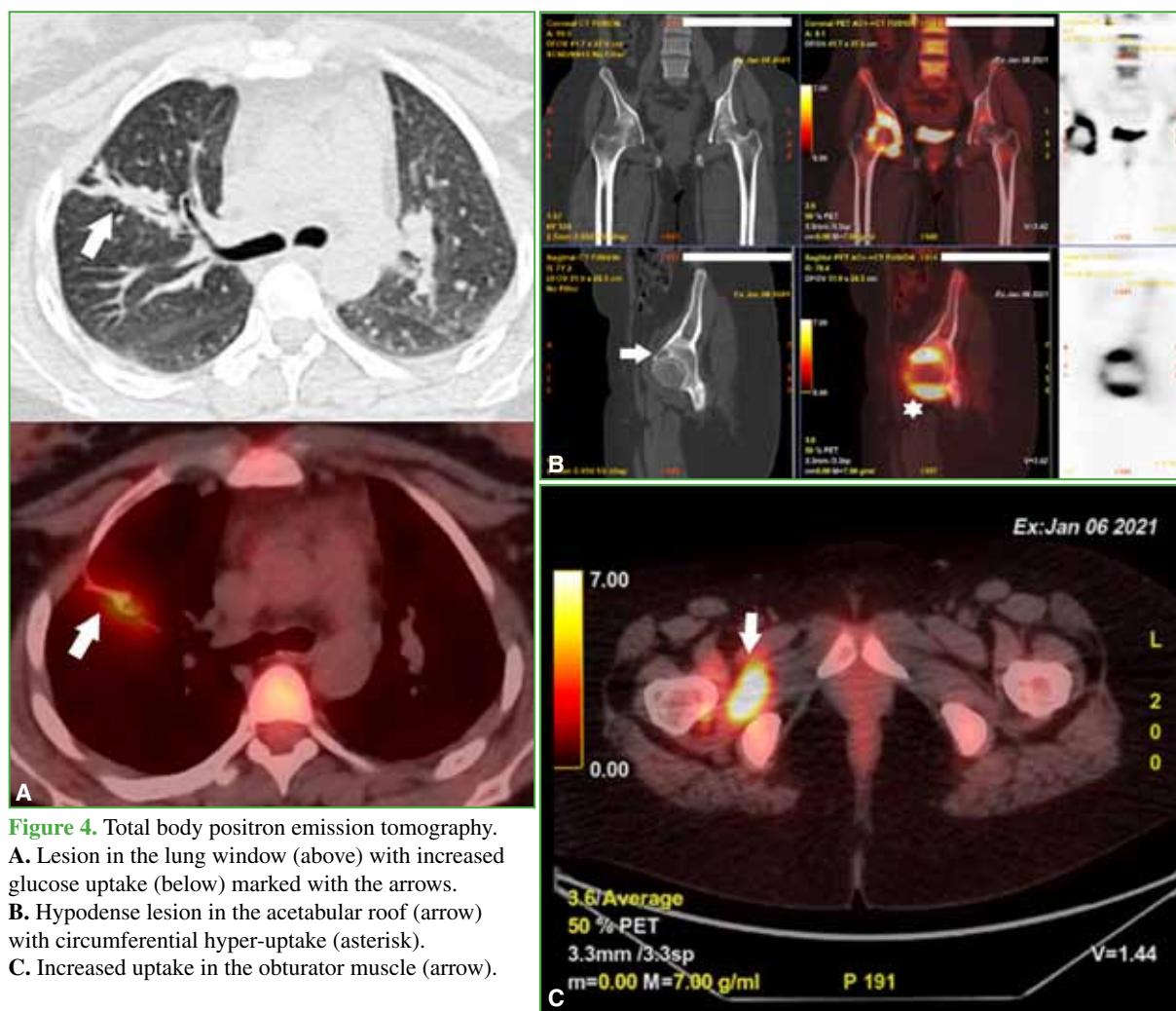


Figure 4. Total body positron emission tomography. **A.** Lesion in the lung window (above) with increased glucose uptake (below) marked with the arrows. **B.** Hypodense lesion in the acetabular roof (arrow) with circumferential hyper-uptake (asterisk). **C.** Increased uptake in the obturator muscle (arrow).

The patient reported that she had had COVID-19 four months earlier. In the workplace, she had had close contact with patients who presented upper respiratory symptoms.

Due to the findings in the magnetic resonance and positron emission tomography, it was decided to perform a CT-guided biopsy of the acetabular lesion (Figure 5).

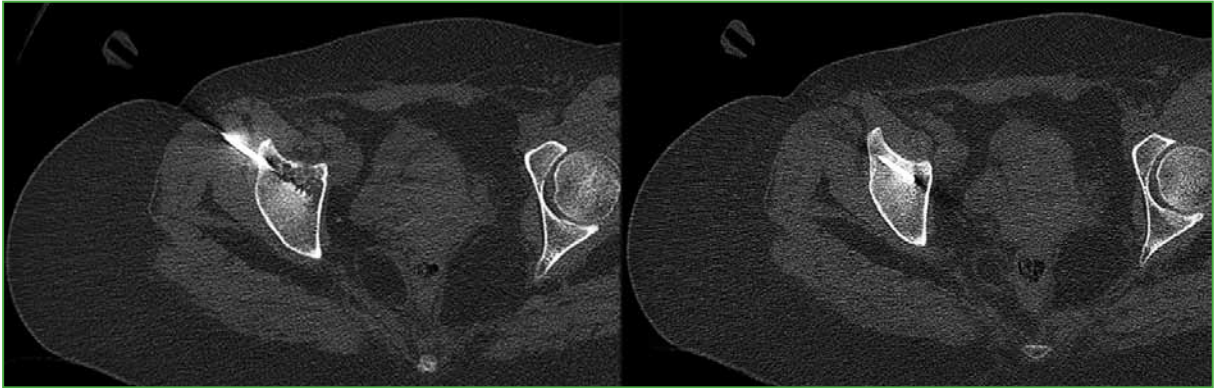


Figure 5. CT-guided biopsy at the level of the acetabulum.

A sample with fragmented trabecular structures that appeared devitalized in sectors was observed in the pathology anatomy study. There were no signs of malignancy.

Because of the lesions seen on the positron emission tomography, the physicians on the tumor committee decided to request a pulmonary evaluation.

The patient was reassessed in the Pulmonology Department; she denied having a systemic history and stated that she did not smoke. A respiratory function test and a chest radiograph were ordered in light of the COVID-19 diagnosis and the positron emission tomography image.

In the functional test, the patient had a restrictive pattern, and the chest radiograph revealed alveolar opacity in the right upper lobe.

With the results of the respiratory evaluation, it was decided to complete the studies with a contrast-enhanced chest CT scan that showed condensation with dense linear trajectories and an air bronchogram, subpleural nodules with a tree-in-bud pattern (**Figure 6**).

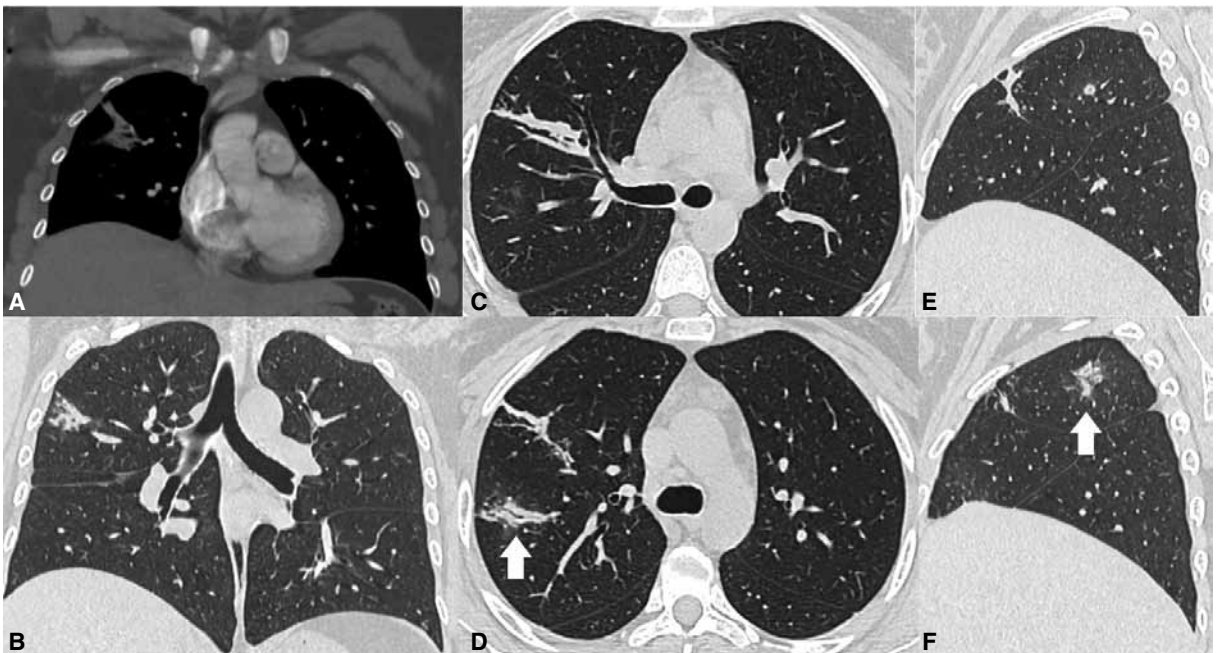


Figure 6. Chest CT scan with contrast. **A.** Mediastinal window in coronal section. Lesion in the right lung field. **B.** Parenchymal window in coronal section. Lesion at the level of the right upper lobe. **C.** Parenchymal window in axial section. Lesion with fibrous tracts and bronchiectasis. **D.** Parenchymal window in axial section. Tree-in-bud patterned lesion (arrow). **E.** Parenchymal window in sagittal section of the right lung with fibrotic lesion. **F.** Parenchymal window in sagittal section of the right lung with a tree-in-bud lesion (arrow).

After ruling out an acute respiratory condition and a neoplastic process in the hip, an interconsultation with the Rheumatology Service was carried out. A new evaluation of the hip with tomography was requested (Figure 7).

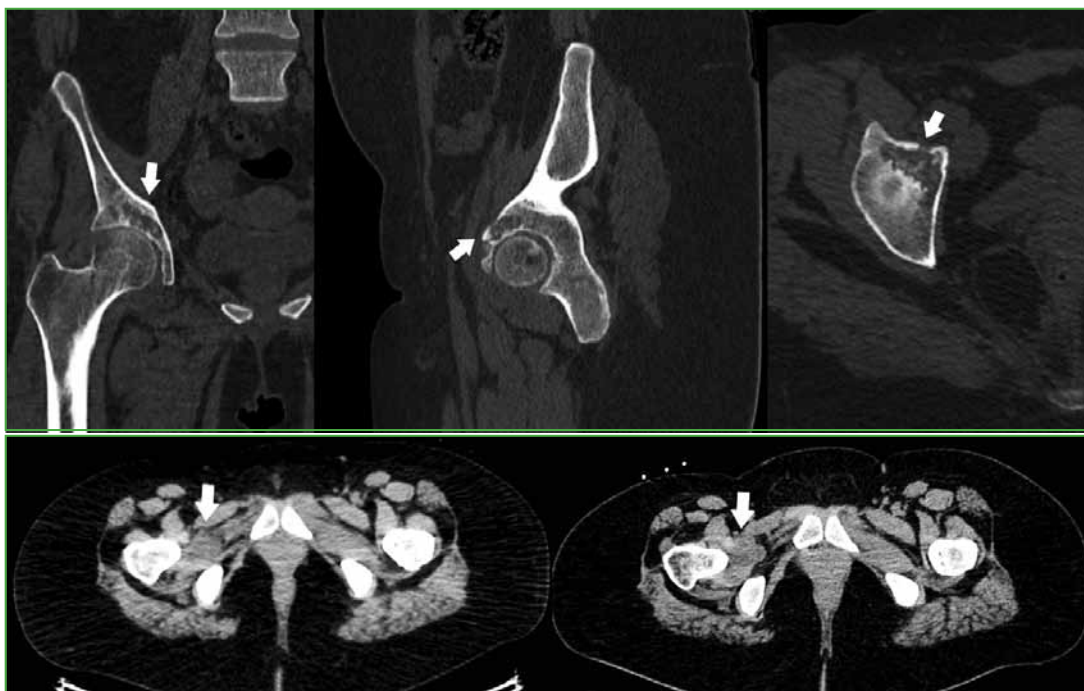


Figure 7. CT scan of the right hip. The progression of the lesion is visualized, now with a lytic component, with compromise of the cortex in the coronal (A), sagittal (B) and axial (C) sections. D. Soft tissue window. When compared to the previous month's study (left), there is a slight increase in the size of the lesion adjacent to the joint (right).

Given the increase in the soft tissue component that surrounds the acetabulum, a new obturator plane biopsy was performed, (Figure 8) with samples sent for bacteriology and pathology analysis.



Figure 8. CT-guided soft tissue biopsy.

The bacteriological study was negative and the anatomical pathology study indicated chronic synovitis with sarcoidosis granulomas.

The poor response to medical treatment led to the indication of a total hip replacement with intraoperative debridement and biopsy (Figure 9). The diagnosis of chronic granulomatous synovitis was confirmed.



Figure 9. Radiograph of the right hip with a total hip replacement.

DIAGNOSIS

With all these findings, musculoskeletal sarcoidosis was diagnosed.

Sarcoidosis is a multisystemic, inflammatory, granulomatous disease of unknown cause, most common in young adults (between 35 and 50 years of age). There is a slight predominance in the female sex. Clinically it can present with pulmonary sarcoidosis, bilateral hilar adenopathy (90%), or extrapulmonary sarcoidosis. It can also affect, in order of frequency, the skin, eyes, and musculoskeletal system (Table).

Table. Manifestations of musculoskeletal sarcoidosis

Joint	Myopathy	Bones
Acute. Rare identification on x-ray Löfgren's syndrome (arthralgia, erythema nodosum, and bilateral hilar lymph nodes) Chronic arthritis, non-deforming granulomatous synovitis, or non-erosive deforming arthritis (Jaccoud's deformity) Dactylitis or tenosynovitis, most common in ankles, knees, elbows, and phalanges Joint impingement is unusual	Diaphragm or extraocular muscles Chronic proximal myopathy or acute simulant polymyositis Nodular (single or multiple painful nodules) Periosteal compromise	More frequent in hands and phalanges Bone destruction in the metaphysis Cystic bone lesions with well-defined margins and lytic bone lesions with periosteal reaction Sclerotic bone lesions Osteopenia or osteoporosis

Diagnosis requires detection of a noncaseating granuloma and compatible presentations after excluding other identifiable causes. It submits spontaneously.

Treatment consists of glucocorticoids or biological drugs.

The most frequent differential diagnoses are neoplastic processes (Figure 10), infections or other granulomatous processes (tuberculosis).



Figure 10. Proliferative neoplastic process. Ewing's sarcoma. A 13-year-old patient with left hip pain of months of evolution. **A.** Panoramic radiograph of the pelvis without particularities. **B.** Computed tomography of the pelvis in bone window, coronal section. A hypodense lesion (arrow) is visualized with septa inside, and bulging and disruption of the cortex. **C.** Computed tomography of the pelvis in bone window, axial section. Cortical disruption is confirmed (arrow). **D.** Magnetic resonance imaging of the pelvis, axial section, in T1-weighted sequence. A hypointense infiltrative lesion is seen in the left acetabulum (asterisk). **E and F.** Magnetic resonance, axial and coronal slices, in STIR sequence. A hyperintense lesion with detachment of the periosteum and involvement of soft tissues is visualized (arrowhead).

S. L. Iglesias ORCID ID: <https://orcid.org/0000-0002-1823-0416>

B. L. Allende ORCID ID: <https://orcid.org/0000-0003-2757-4381>